Available online at www.sciencedirect.com

ScienceDirect

Ciência & Tecnologia dos MATERIAIS

http://ees.elsevier.com/ctmat

Ciência & Tecnologia dos Materiais 29 (2017) e71–e75

Special Issue "Materiais 2015"

Study of nanomechanical properties of (1-*y*)BST-*y*MgO thin films

Dionizy Czekaj[a, *], Agata Lisińska-Czekaj[a], Julian Plewa[b]

[a]*University of Silesia in Katowice, Institute of Technology and Mechatronics, 12 Żytnia St., Sosnowiec 41-200, Poland*
[b]*University of Applied Sciences Münster, Department of Chemical Engineering, Stegerwaldstrasse 39, D-48565, Steinfurt, Germany*

Abstract

In the present study thin films of MgO – modified $Ba_{0.6}Sr_{0.4}TiO_3$ (BST60/40) solid solution were prepared by the sol-gel-type chemical solution deposition method on stainless steel substrates. A multilayer spin-coating approach was utilized for the $Ba_{0.6}Sr_{0.4}TiO_3$-MgO thin film deposition with subsequent thermal annealing at T=650-750°C. Dried BST60/40-MgO gel powders were studied with thermogravimetric and differential thermal analysis to determine their thermochemical properties. X-ray diffraction analysis was utilized for thin film characterization in terms of its phase composition and crystal structure. The influence of y=1, 3 and 5 mol.% MgO doping on nanomechanical properties of BST60/40 thin films was studied with nanoindentation. It was found that BST6040 thin films adopted the tetragonal *P4mm* (99) structure. The volume of the BST60/40 elementary cell, the average hardness as well as the mean value of the Young modulus decreased with an increase in amount of MgO.

Keywords: BST thin films; sol-gel method; crystal structure; AFM; nanoindentation.

1. Introduction

Ferroelectric thin films of barium strontium titanate ($Ba_{1-x}Sr_xTiO_3$) have been of great interest for their application in dynamic random access memories (DRAM), infrared sensors, electro-optical devices and also in electrically controlled microwave devices for wireless communication. Electrical and optical properties, such as high dielectric permittivity, low dielectric losses, large electro-optical coefficient and low optical losses, are critical for these applications [1]. In case of application of electrically controlled (i.e. "tunable") microwave devices as phase shifters, filters, steerable antennas, varactors, etc. in practice, both ferroelectric and paraelectric phases may be useful [2]. However, it should be noted that the paraelectric phase is often preferred for application in microwave device technology since it has no hysteresis associated with the ferroelectric domain walls movement [3].

It is commonly known [4,5] that the Curie temperature (T_C) of $Ba_{1-x}Sr_xTiO_3$ solid solution can be controlled by adjusting the Ba/Sr ratio. It varies from T_C≈120-130°C to T_C≈-240°C for x from 0.0 to 1.0. So, the Curie point can be close to the room temperature for Ba/Sr ratio to be 73/27.

Despite widespread investigations of several different properties of $Ba_{1-x}Sr_xTiO_3$ thin films, there is still lacking sufficient research systematically correlating the mechanical and structural relationships on a nanometre-scale for designing advanced electronic devices. It is essential that studies continue on the mechanical characterization of these thin films to recognize how the relative parameters affect the material structure and the properties for use in advanced applications [6].

Goal of the present studies was to deposit $Ba_{0.6}Sr_{0.4}TiO_3$ (BST) thin films doped with 1, 3 and 5 mol.% MgO on polished stainless steel substrates by sol-gel method and to reveal the influence of MgO

* Corresponding author.
E-mail address: dionizy.czekaj@us.edu.pl (D. Czekaj)

http://dx.doi.org/10.1016/j.ctmat.2016.07.017

dopant on microstructure, crystal structure and mechanical properties of BST thin films.

2. Experimental

Details of the thin film deposition technology were given by us elsewhere [7,8]. Let us only mention that the precursor solution prepared on the base of barium acetate, strontium acetate, magnesium acetate and tetra-butyl titanate was deposited by spin coating on polished stainless steel substrates (AISI 304 type). The wet films were given a two-stage heat treatment at T=150°C and at T=350°C for t=5 min. The coating process was repeated up to 30 times. Final crystallization of as-deposited BST thin films was carried out in an ambient atmosphere at T=650–750°C for *t*=2h by conventional furnace annealing.

Simultaneous thermal analysis (STA), including both differential thermal analysis (DTA) and thermogravimetry (TG), was used to investigate thermal effects in the dried gel powders. The measurements were performed with Netzsch STA409 thermal analyser.

The crystal structure of ceramic thin films was studied by X-ray diffraction method at room temperature (XPert–Pro diffractometer, Θ - 2Θ mode, CoKα radiation, data angle range, 2Θ=10-105° and detector scan step size $\Delta 2\Theta$=0.01°; scan type continuous and scan step time t=7s). The phase and structural analysis was performed with X'pert HighScore Plus software (PANalytical B.V) and the latest available ICSD [9], database was utilized. Refinement of the structural parameters of BST phase was performed with the Rietveld method [10].

Nanomechanical properties of BST – MgO thin films were determined using a nanoindenter (Hysitron Triboscope, USA) with a three-sided pyramidal Berkovich indenter tip for all indentation testing, performed at room temperature. For each specimen, a maximum indentation load of F_L=500 μN and a loading time of t_L=1, 2 and 11s were used. The nanoindenter was equipped with an atomic force microscope (AFM) thus enabling the surface characterization. Calculations of geometric parameters characterizing the grain-size distribution were performed with XEI, an Image Processing Program for SPM data (by PSIA Inc, now Park Systems [11]).

3. Results and discussion

3.1. Thermal analysis

An example of thermal evolution of BST60/40 dried gel modified with 1 mol.% MgO is shown in Fig. 1.

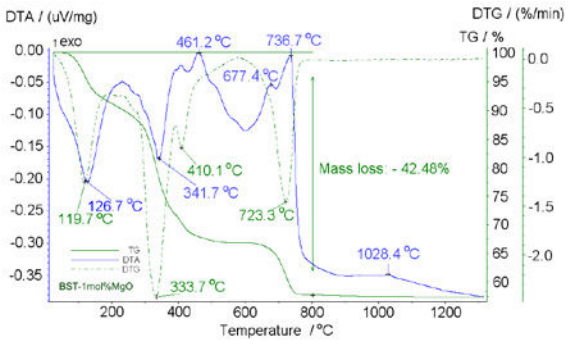

Fig. 1. Thermal evolution of BST60/40-1 mol.% MgO dried gel.

One can see that TG curve is characterized with a large three-staged mass loss Δm> 42% [12]. The first drop of the TG curve was due to the evaporation of solvents. One may also see the endothermic peak on DTA curves at T≈127°C corresponding to the weight loss on the TG curves. The notable weight loss was detected at T≈400°C, which matched an endothermic peak on the DTA curves at T≈342°C. Since no crystallization takes place below T=500°C, the weight loss is probably due to the decomposition of organic additives in the gel. The exothermic peak around T≈460°C could be due to crystallization of various intermediate phases. It is known that, for sol-gel derived barium titanate, several intermediate phases form prior to the transformation of the amorphous phase into the perovskite phase. The nature of these intermediate phases and the crystallization sequence depend upon the precursors used [13].

The third drop takes place between T=650°C and T=750°C. It corresponds to relatively broad exothermic features at T≈677-680°C, and T≈733-737°C on the DTA curve. From the XRD measurements the growth of perovskite BST was ascertained. The weight loss originates from the release of various side products [12].

3.2. X-ray analysis

X-ray diffraction patterns of the stainless steel substrate and MgO modified BST60/40 thin films are shown in Fig. 2.

One can see in Fig. 2 that contribution of stainless steel substrate is visible in the diffraction patterns of

BST60/40 thin films at the angle $2\Theta \approx 51.05°$, 59.73° and 89.56° (iron nickel, ICSD code 632933).

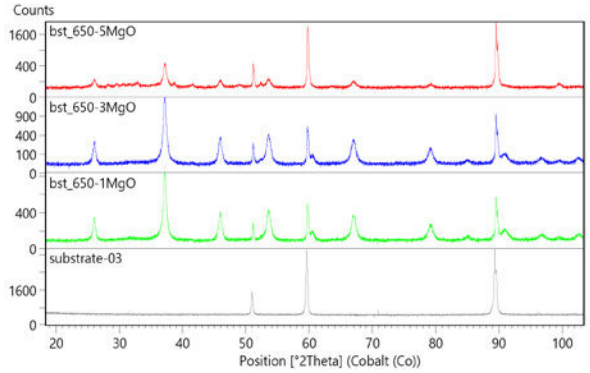

Fig. 2. X-ray diffraction patterns of MgO – doped BST60/40 thin film grown by sol-gel method on stainless steel substrate (bottom curve) and annealed at T=650^{0}C.

Results of the X-ray diffraction phase and structural analysis are shown in Fig. 3 where data for BST60/40 thin film doped with 3%mol. MgO are presented.

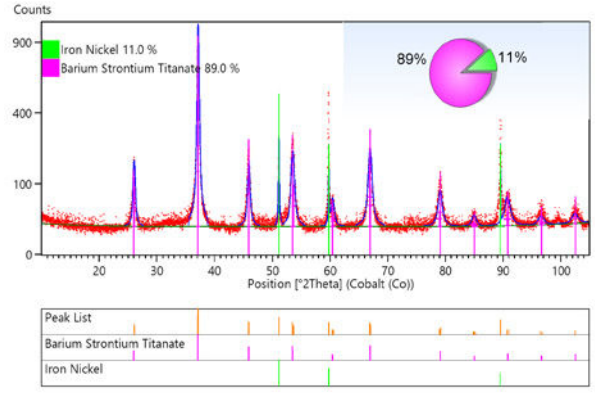

Fig. 3. Results of phase and structural analysis of X-ray diffraction pattern recorded for 3%mol. MgO – doped BST60/40 thin film grown on stainless steel substrate and annealed at T=650^{0}C.

According to the search and match procedure the BST phase was retrieved (ICSD code 54150). Model of the crystal structure of the BST phase was first of all modified (i.e., occupancy of Ba/Sr sites was changed) and after that it was used for the Rietveld refinement. Refined structural parameters of the MgO-modified BST60/40 phase (annealed at T=650°C) are given in Table 1.

Results of the calculations (Table 1) showed that BST60/40 thin films adopted the tetragonal *P4mm* (99) structure. However, volume of the elementary cell increases with an increase in amount of MgO.

Table 1. Structural parameters of BST60/40 phase.

Relevant parameters of BST phase	BST60/40-1% MgO	BST60/40-3% MgO	BST60/40-5% MgO
Lattice parameters	Space group (No.)		
	P4mm (99)	*P4mm* (99)	*P4mm* (99)
a (Å)	3.978	3.981	3.983
b (Å)	3.978	3.981	3.983
c (Å)	3.965	3.965(1)	3.971
V (10^6 pm^3)	62.74	62.82	62.98

It is worth noting that such structural defects like oxygen vacancies decrease forces of the Coulomb attraction between anions and cations in their close neighbourhood thus causing an increase in interatomic distances which, in turn, leads to an increase in volume of the elementary cell. Therefore, the observed expanding of the elementary cell may suggest that concentration of oxygen vacancies increases with an increase in amount of MgO dopant in BST60/40 thin films.

3.3. Results of the grain analysis for BST thin films

Results of the grain analysis performed with AFM are shown in Table 2. One can see that for BST thin film doped with 3 mol.% of MgO the mean geometric parameters characterizing the grain-size distribution attained the local minimum.

Table 2. Mean values of the geometric parameters characterizing the grain-size distribution of BST60/40 thin films doped with 1, 3 and 5 mol.% MgO (from AFM measurements).

Relevant parameters of BST phase	BST60/40-1%MgO	BST60/40-3%MgO	BST60/40-5%MgO
Mean area (μm^2)	0.2111	0.1173	0.134
Mean volume (μm^3)	0.0368	0.01992	0.02877
Mean dimension (μm)	0.733	0.533	0.555
Mean perimeter (μm)	2.176	1.603	1.674

Influence of the amount of MgO on the average crystallite size was evaluated on the base of broadening of the diffraction lines with the help of the Scherrer equation [14]. Five diffraction lines were first fitted with the Gauss function and then a contribution of the diffraction line broadening to the crystallite size was extracted. Results showed that for MgO amount of 1, 3 and 5 mol.% the average crystallite size of BST60/40 phase was $<D_1>$=23 nm, $<D_3>$=27 nm, and $<D_5>$=34 nm, respectively.

Referring to the above mentioned results, it is worth noting that the surface topography evolution of the sol-gel derived thin film depends on agglomeration

mechanisms of the primary particles. Nanosized primary particles differ from coarser particles by their increasing tendency to form agglomerates (i.e., the smaller the size the higher the tendency). Aggregates develop when primary particles begin to form a common crystalline structure [15]. Agglomerates or aggregates are macroscopically perceived as one particle. Therefore, taking into consideration that crystallites (characterized by X-ray diffraction method) are primary particles and that grains (observed by AFM) are aggregates of primary particles, the results on influence of MgO content on grain size and crystallite size are consistent with each other: the smaller the amount of MgO, the finer the average crystallite size; the higher the tendency to form agglomerates, the higher the mean dimension of the grains.

Quality of the crystal structure of BST thin films was evaluated in terms of microdeformations. It was found that MgO modifier decreased quality of the crystal structure: micro strains increased with an increase in amount of MgO and reached value of 0.31%, 0.32% and 0.40% for 1, 3 and 5 mo.%, respectively.

3.4. Results of the force-displacement measurements

Modern nanoindentation testing equipment allows penetration depth curves to be measured as a function of load where the loads extend down to the range of micro-Newtons, resulting in typical penetration depths in the range of nanometres. This technique is well suited for examining the mechanical properties of thin films [6].

An example of a load-penetration depth curve is shown in Fig. 4.

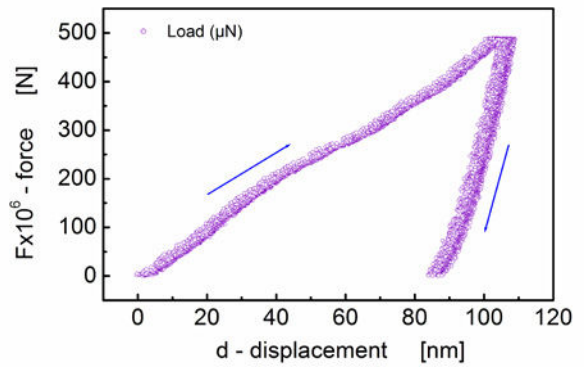

Fig. 4. An example of a load-penetration depth curve for BST60/40 thin film.

It should be noted that hardness (H) and elastic modulus (E) were determined by means of the method of Oliver and Pharr [16,17], and the Poisson's ratio of the thin films was assumed to be σ=0.3 for calculating the thin film's Young's modulus.

Parameters from that particular measurement were as follows: elastic modulus E=132.93 GPa, hardness H=8.17 GPa, contact depth d_C=97.3 nm, contact stiffness k_C=36.6 μN/nm, maximum force F_{max}=487.1 μN, maximum depth d_{max}=109 nm, contact area S=59613.1 nm^2.

Results of the performed measurements and calculations are given in Fig. 5.

One can see in Fig. 5 that for BST – MgO thin films grown on stainless steel substrates the average hardness decreases with an increase in the amount of the acceptor admixture from H=10.14 GPa for 1% MgO – doped to H=6.71 GPa for 5% MgO – doped BST6040 sol-gel derived thin film. Mean value of the Young modulus also decreases with an increase of MgO content from E=150 GPa to E=85 GPa for 1% and 3% of MgO, respectively.

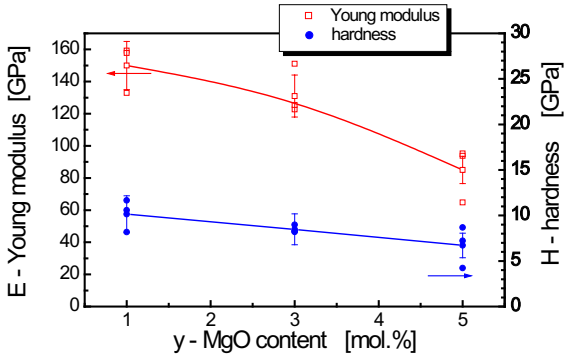

Fig. 5. Hardness and Young modulus of MgO – doped BST6040 thin films

4. Conclusions

On the base of thermal analysis of parameters of the heat treatment of sol-gel derived BST thin films were determined. It was found that BST6040 thin films annealed at T=650°C adopted the tetragonal structure described with *P4mm* (99) space group. The volume of the BST60/40 elementary cell as well as the average crystallite size and micro strain were found to increase with an increase in amount of MgO. Decrease in quality of the crystal structure caused a decrease in the average hardness as well as the mean value of the Young modulus.

Acknowledgements

The present research was supported by University of Silesia in Katowice, Poland from the funds for science – research potential (NO 1S-0800-001-1-05-01).

References

[1] D. Czekaj, Fabrication and study of BST – based functional materials, University of Silesia, Gnome Publishing House, Katowice, Poland, 2010, p. 122.
[2] N. Setter, D. Damjanovic, L. Eng. G. Fox, S. Gevorgian, S. Hong, A. Kingon, N.Y. Park, G.B. Stephenson, I. Stolitchinov, A.K. Tagantsev, D.V. Taylor, T. Yamada, S. Streiffer, J. Appl. Phys. 100 (2006) 051606.
[3] O.G. Vendik (Ed.), Segnetoelektriki v Tekhnike SVCH, Moskva, Sov. Radio., 1979.
[4] B. Jaffe, W.R. Cook, H. Jaffe, Piezoelectric Ceramics, Academic Press, London, 1971.
[5] J-H. Jeon, J. Eur. Ceram. Soc. 24 (2004) 1045.
[6] Sheng-Rui Jian, Win-Jin Chang, Te-Hua Fang, Liang-Wen Ji, Yu-Jen Hsiao, Yee-Shin Chang, J. Mater. Sci. Eng. B 131 (2006) 281.
[7] D. Czekaj, A. Lisińska-Czekaj, J. Adv. Dielectr. 2(1) (2012) 1.
[8] A. Lisińska-Czekaj, J. Orkisz, T. Orkisz, D. Czekaj, Ceram. Mater. 67(1) (2015) 48.
[9] ISCD Database, FIZ Karlsruhe, <http://www.fiz-karlsruhe.de>, 2015 (accessed 22.06.2015).
[10] H.M. Rietveld, Aust. J. Phys. (1988) 113.
[11] Park Systems http://www.parkafm.com/, 2015 (accessed 29.06.2015).
[12] K. Osinska, D. Czekaj, J. Therm. Anal. Calorim. 113 (2013) 69.
[13] S.B. Majumder, M. Jain, A. Martinez, R.S. Katiyar, F.W. Van Keuls, F.A. Miranda, J. Appl. Phys. 90(2) (2001) 896.
[14] A.L. Patterson, Phys. Rev. 56 (1939) 978.
[15] D. Walter, Deutsche Forschungsgemeinschaft (Ed.), Nanomaterials, Wiley-VCH Verlag, Weinheim, Germany, 2013, pp. 1-24.
[16]W.C. Oliver, G.M. Pharr, J. Mater. Res. 19(1) (2004) 3.
[17] L. Prchlik, J. Mater. Sci. 39 (2004) 1185.